

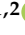



Article

Experimental Implementation of Power-Split Control Strategies in a Versatile Hardware-in-the-Loop Laboratory Test Bench for Hybrid Electric Vehicles Equipped with Electrical Variable Transmission

Majid Vafaeipour ^{1,2} , Mohamed El Baghdadi ^{1,2}, Florian Verbelen ^{2,3}, Peter Sergeant ^{2,3} , Joeri Van Mierlo ^{1,2}  and Omar Hegazy ^{1,2,*} 

- ¹ ETEC Department & MOBI Research Group, Vrije Universiteit Brussel (VUB), Pleinlaan 2, 1050 Brussel, Belgium; majid.vafaeipour@vub.be (M.V.); Mohamed.El.Baghdadi@vub.be (M.E.B.); Joeri.Van.Mierlo@vub.be (J.V.M.)
- ² Department of Electromechanical Systems and Metal Engineering, EEDT Group, Ghent University, 9052 Ghent, Belgium; Florian.Verbelen@UGent.be (F.V.); Peter.Sergeant@UGent.be (P.S.)
- ³ Flanders Make, 3001 Heverlee, Belgium
- * Correspondence: Omar.Hegazy@vub.be

Received: 25 May 2020; Accepted: 14 June 2020; Published: 21 June 2020



Abstract: The energy management strategy (EMS) or power management strategy (PMS) unit is the core of power sharing control in the hybridization of automotive drivetrains in hybrid electric vehicles (HEVs). Once a new topology and its corresponding EMS are virtually designed, they require undertaking different stages of experimental verifications toward guaranteeing their real-world applicability. The present paper focuses on a new and less-extensively studied topology of such vehicles, HEVs equipped with an electrical variable transmission (EVT) and assessed the controllability validation through hardware-in-the-loop (HiL) implementations versus model-in-the-loop (MiL) simulations. To this end, first, the corresponding modeling of the vehicle components in the presence of optimized control strategies were performed to obtain the MiL simulation results. Subsequently, an innovative versatile HiL test bench including real prototyped components of the topology was introduced and the corresponding experimental implementations were performed. The results obtained from the MiL and HiL examinations were analyzed and statistically compared for a full input driving cycle. The verification results indicate robust and accurate actuation of the components using the applied EMSs under real-time test conditions.

Keywords: hybrid electric vehicle (HEV); hardware-in-the-loop (HiL); model-in-the-loop (MiL); software-in-the-loop (SiL); equivalent consumption minimization strategy (ECMS); low pass filter (LPF); electrical variable transmission (EVT); embedded software

1. Introduction

The need for the reduction in our carbon footprint has coincided with upward fuel prices, which has prompted an increased focus in the search for energy-saving solutions related to the transportation sector. Hence, unleashing the maximum potential of hybrid and electric vehicles at different fleet and standalone energy management design levels is at the forefront of research in the automotive industry [1–3]. The energy management strategy (EMS) unit is the heart of power sharing control toward addressing the consumption-friendly objectives of electric vehicle design. Compared to their conventional counterparts, hybrid electric vehicles (HEVs) can offer lower fuel consumption and still provide a similar/enhanced performance. However, as HEVs usually comprise

two or more energy supply sources, developing their architectures with an efficient EMS involves a plethora of complexities related to design, integration, and implementation. Due to these cost-effective complexities, the plausibility of any control strategy requires assessment through various testing and validation procedures before embedment in the electronic control unit (ECU) of an on-road vehicle [4]. In this regard, the response and accuracy of a control strategy is of great significance for extensive verification through the use of a complete chain of tools. Toward real-world applicability, the model-based design of a plant and its EMS include various steps from the development to validation phases. This generally starts with functional system definitions and ends with deploying the design to a real operating environment under offline system modeling, control algorithm synthesis, simulation analysis, and online vehicle implementations [5]. To this end, first, a model-in-the-loop (MiL) development must be performed in which the integrated plant and the corresponding EMS controller models are built and set up in a desktop environment (i.e., MATLAB/Simulink®) to be examined over a complete driving cycle. This considers a totally software-based and iterative trial and error approach toward achieving an initial design with good flexibility and low cost in a short period [6]. In this phase, it is possible to perform fast EMS design alternations to investigate corresponding effects on a set of predefined objectives.

Thereafter, through software-in-the-loop (SiL) evaluations, one can test the plant and controller models in a slightly more realistic environment as the corresponding C/C++ code can be generated for digital implementation tests. The possibility of design modification in this stage is slower time-wise as there is a need to go back, modify the initial model, and regenerate the C/C++ code if required. This step is of great importance to test the feasibility of the built code in terms of real-time evaluation. In this regard, convertibility of the control algorithms to C/C++ code assures that they are downloadable into digital signal processing (DSP) boards (e.g., dSPACE rapid prototyping product, “MiroLab Box”) for processor-in-the-loop (PiL) tests as a next phase. The PiL phase considers hardware features and provides realistic situations by running the control algorithm for an emulated target behavior [7]. Hence, these steps can not only reveal coding failures, but also provide helpful insights for the hardware-in-the-loop (HiL) implementation where the vehicle behavior can be reproduced.

In the HiL phase, the developed control algorithms with mathematical models running in real-time can be fully installed on a control hardware to communicate and actuate real/emulated components. A typical HiL system integrates various software and hardware-based units such as physical components (not in all testbeds), component emulators, DSP/FPGA unit, MATLAB/Simulink® desktop environment, real-time interface (RTI), real-time workshop (RTW), and controller area network (CAN) [8]. In the HiL implementation stage, exerted road load on wheels can be manipulated in a real-time manner by introducing an input driving cycle to the physical testbed to examine operating conditions as if in a real driving environment. The main objective of HiL implementation is to experimentally test and verify the feasibility, accuracy, high dynamic response, scalability, and reliability merits of a designed control algorithm to guarantee its real-world applicability. The HiL test ensures savings in design cost and time by reducing the total development cycle of vehicle calibration as it indicates how an EMS control unit, and consequently the plant’s components, will communicate and behave in a real vehicle. In other words, it provides a validation method for development engineers for the safety and precision of the control system before an actual mule vehicle is available. Hence, once an EMS is designed and verified in a closed-loop manner through HiL, it can ideally be transmitted to a vehicle-in-the-loop (ViL) testbed without design modifications, expecting that the proposed strategy can represent identical features. Considering the discussed phases, Figure 1 recapitulates the chronological design steps known as the “V” development process [7].

Although the effectiveness of various EMS algorithms has been extensively reported in previously performed studies, many have been limited to an early EMS design stage (i.e., MiL) of the studied topologies. There has been a tremendous interest in the development of these virtually tested models mainly based on optimization-based (OB) and rule-based (RB) techniques, but in the absence of real-time implementation. Instead, the main outcomes have compared the validity and competency of

approaches in addressing the non-linearities/multimodalities of non-convex objectives such as fuel consumption enhancement and battery charge-sustaining in a fully software-based way. For example, in [9], objectives such as battery charge-sustaining and improving fuel economy were considered using a RB EMS, and power distribution through the vehicle components were investigated. In another study [10], different RB strategies were compared in terms of fuel consumption improvements, and the computational costs of the RB EMSs were evaluated through a comparison for a use-case of parallel HEV topology in [11]. In another study [12], the battery state of charge (SoC) control, power flow, and fuel consumption were evaluated through a RB power split method considering the engine operating points. The SoC pattern evolutions were investigated in [13] using a RB supervisory control approach, and in [14], a driving cycle recognition method was employed to improve fuel efficiency. Huang et al. [15] performed an optimization of the control strategy parameters for a series HEV topology to minimize the fuel consumption. In that study, different OB techniques were compared for optimal EMS design in a MATLAB/Simulink® environment where the results indicated the superiority of genetic algorithm (GA) compared to DIRECT and thermostatic (On/Off) methods. In another study, Montazeri and Poursamad [16] proposed an OB EMS of HEVs by aggregating the constraints into the objective function. In that study, penalty functions were used to weed out the infeasible solutions and minimize fuel consumption and emissions. Gao et al. [17] used GA in a PSAT environment for powertrain optimization of a parallel HEV topology to improve the overall fuel economy. Salmasi [18] for HEVs and Martinez et al. [19] for plug-in HEVs classified and overviewed control strategies including various RB and OB methods, leading to future trends in the field. The equivalent consumption minimization strategy (ECMS) was incorporated into driving cycle prediction, performing horizon optimizations, and pattern recognition concepts in [20,21] to provide efficient power splitting. Along the same line, ECMS approaches have been proposed that rely on considering instantaneous SoC values to be used as state feedback to control the battery SoC variation for charge-sustaining [22–24].

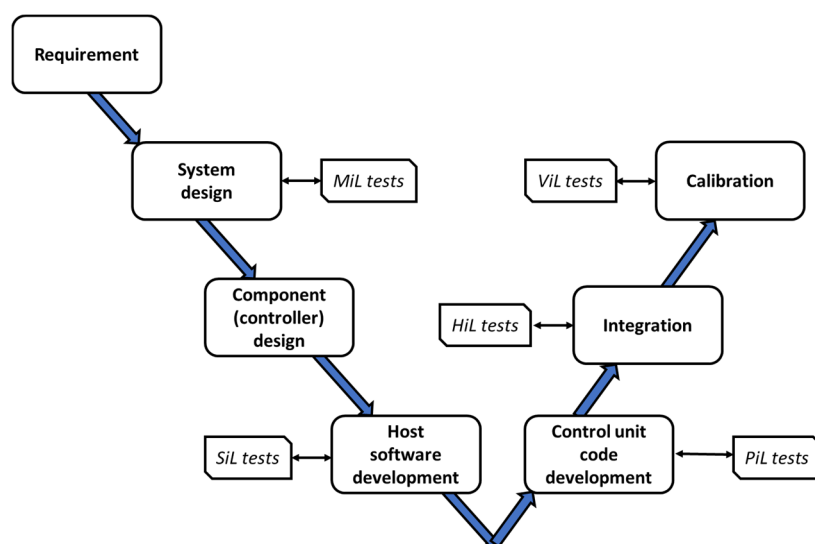


Figure 1. The “V” development process composed of various testing phases.

In contrast to the above-mentioned studies, researchers have taken investigations to a next level by carrying out experimental examination of EMSs through HiL tests to address their real-time performance and applicability. However, among these studies, many have been limited in terms of including testbeds that can represent a drivetrain architecture in a high-fidelity manner. In other words, in these test benches, fast prototyping of equivalent drivetrains by using hardware-based simulators/interfaces were considered instead of including mechanical (e.g., rotatory machines) and electrical (e.g., battery, inverters, and converters) prototyped components. For example, in [8], a HiL

test system without prototyped components and based on a standalone dSPACE and control desk was employed to verify the real-time capability of an ECMS-based approach versus the simulation results proposed for a hybrid city bus. In another study, the typical control strategies of two passenger HEVs, a Jeep Commander and Toyota Prius, were tested through a university HiL testbed with limitations on the maximum torque and speed measurement [25]. In that test bench, the objective was to combine relatively low-cost off-the-shelf products to examine the test environment and realize phases of real-time data acquisition, signal generation, automatic code generation, and power measurements using MATLAB/Simulink®, dSPACE, and a Hioki power analyzer. The applicability of combining RB and OB EMS control were proposed in [26], while the experimentally-determined parameters of the components were considered instead of real drivetrain components for considering motor/generator dynamics and battery. Li et al. [5] performed a HiL analysis for EMS of a parallel HEV by a rapid prototyping approach. They investigated low-level ECUs coupled to a dSPACE HiL simulator to virtually capture and actuate signals for the engine and motor's torque-speed operating pairs over a full driving cycle. Wu et al. [27] combined embedded and software-based simulations to verify the feasibility of a HiL methodology for a supervisory control downloaded into a midsize HiL machine including a load emulator card. This semi-physical study was performed based on a practical application of dSPACE products to provide ECU development as a progress phase. In that study, it was reported that including other physical units to their test bench was required for further realistic verification tests. The components of a series-parallel hybrid electric city-bus were modeled in MATLAB/Simulink® by Wang et al. [28] and its EMS was tested. In that study, a commercial HiL simulator, PT-LABCAR, in the presence of a real control unit, were used, while the engine, motor, and battery were emulated in a software-based manner. To verify the control, the actual and setpoint speed of the final drive were compared. However, similar comparisons are essential for other crucial features (i.e., torque and rotational speed) to confirm the controllability, power sharing competency, and actuation response of an EMS in a more comprehensive way. The torque and speed of the engine and motor obtained from the HiL and MiL tests were compared for real-time verification of EMS control for a GM Chevrolet Volt case study by Algarny et al. [29]. The objective of their study was to validate the physical control signals generated by EMS while the components were emulated by mathematical models. In that study, a low-level simple HiL test bench including a TI controller and oscilloscope were used where Typhoon HiL, aside from the PSIM software environments, were used as the interface and model generator, respectively. Chako et al. [30] used a custom real-time simulator platform and a DSP control card to introduce a HiL testbed for the academic development of control algorithms where a Simulink® coder was used for real-time testing of a generated C code. The main objective of that study was only to test the control bench and generate measurable signals for features such as vehicle speed, acceleration, and power at the wheels. In another study [31], a HiL module setup was tested for an inverter ECU and a software-based electric motor for HEVs. In that study, only the control board of the Inverter ECU (HIL Box) was physical, while the remaining components (i.e., HV battery, sensors, DC-link capacitor, electric motor, IGBT-based power electronics board, and drive load) were completely modeled in the MATLAB/FPGA environment.

Compared to the above-mentioned studies, considerable efforts have also been reported in the literature, which have taken verification tests to a more realistic and accurate level by adding up more physical degrees. In contrast to the semi-physical HiL test environments discussed, there have been studies that have included real prototyped components to provide more real-world and versatile test benches. These studies have focused on examining the mechanical/electrical actuation performance of components under real-time operations. Clearly, such a feature facilitates the testbed to include the existing losses of a system more accurately leading to reliable results from the setup. For example, Hui et al. [6] presented a testbed including real components (i.e., internal combustion engine (ICE) and electric motor) for HiL implementation of HEV drivetrains while the battery and gearbox were realized by software models. Their ideally designed testbed employed an electromagnetic clutch, making the testbed switchable between series and parallel configurations. In another real-time study,

Mayyas et al. [32] examined ECMS-based and rule-based power splitting approaches in a roller bench emulating the driving cycle. In that study, the ICE and chassis system were integrated to become a part of a parallel HEV HiL testbed. The experimental HiL system in [33] coupled a real engine with mathematical models of electric systems to verify the implementation of an ECMS-based control through comparisons of the MiL and HiL results for the engine torque. The behavior of fuel cell (FC) and super capacitor (SC), as real components of a multi-source HiL testbed, was assessed by Castings et al. [34,35], while battery and traction load parts were virtually emulated by a current source. The real-time system controllability was validated for an OB strategy in both of these studies. Allegre et al. [36] reported a HiL implementation of an EV with real hybrid energy storage components comprising a battery and SC coupled into dSPACE and emulation choppers. Their experimental results validated the applicability of a low pass filter power sharing method considering a reduced-scale power.

As discussed in the current section, most studies have implemented HiL tests focusing on conventional HEV topologies such as series, parallel, and series-parallel. However, a very limited number of studies have reported on the HiL verification tests of EMSs for a recently promising topology of vehicles: HEVs equipped with EVT. For such a topology, most of the existing studies have reported offline results without assessing the system either in an experimental or realistic environment. In this regard, the EMSs for the power sharing control of EVT-based HEV topologies solely relying on MiL simulations were investigated in [37–39]. On the other hand, there is experimental research that has focused on real-time implementations, but their objectives were limited to the design, testing, and optimization of EVT itself as a component [40–43], rather than on the verification of EMS and system controllability. From a system perspective and to provide a testbed for studying EVT-based HEVs, a scaled HiL platform for real-time implementation was introduced in [44]. However, that study only focused on the feasibility of load emulation where no MiL vs. HiL EMS verification was involved. In another similar study using an identical testbed, an ICE load emulation feasibility study was carried out to emulate the engine's dynamical torque characteristic for a limited time section of a driving cycle [45]. The complexities due to the electromagnetic features of an EVT makes reliable modeling and simulation of EVT-based powertrains a challenging task. Thus, for such HEV systems, performing MiL versus HiL investigations is of great importance to validate the applicability of a design, specifically from dynamic controllability aspects over the different conditions of a complete driving cycle.

Compared to the literature thoroughly reviewed in the current section, the main contribution of the present work can be described as follows:

- It focuses on both MiL and real-time HiL examinations for a less-extensively studied topology, EVT-based HEVs.
- It involves real components of the topology prepared in an innovative HiL test bench for performing reliable verification tests of the employed EMSs.
- It validates the real-time actuation of the components over the existing dynamics of a full driving cycle.

To these ends, the whole vehicle and corresponding optimized EMS subsystems were first modeled and simulated in the MATLAB/Simulink® environment. Thereafter, associated HiL tests were experimentally performed in the experimental setup. The dynamic agreements of torque and speed achieved from the MiL and HiL tests were compared and statistically analyzed to validate the EMSs' applicability and power split competencies. Accordingly, the remainder of the paper is organized as follows. Section 2 presents the EVT-based drivetrain architecture for a passenger HEV. In Section 3, the individual mathematical modeling of the vehicle components and corresponding descriptions are elaborated. Section 4 provides the formulation and explanations of the employed EMSs and their incorporation into the model for off-line optimization. Section 5 presents the specifications of the prepared experimental testbed and its featuring advantages. In Section 6, the study procedure is provided, and the statistical performance indices required for the agreement and error analyses

are briefly expressed. Section 7 presents and discusses the obtained verification results, and finally, Section 8 recapitulates the achieved outcomes and provides the conclusions and future work directions.

2. Electrical Variable Transmission (EVT)-Equipped Hybrid Electric Vehicles (HEV) Architecture

Due to their unique electromechanical features, electrical variable transmission (EVT) devices offer opportunities as a substitute solution to conventional transmission systems. The EVT encompasses two concentric rotors, an inner and outer, which are nested in a stator frame for mechanical, electrical, and electromagnetic energy exchange and transfer [46,47]. This makes EVT a suitable choice for use in applications where continuously variable and electric drive are combined with power generation components to provide improvement in overall efficiency and functionality. Example applications include but are not limited to transmission systems in hybrid electric vehicles (HEV), constant speed power take-off with mechanical drive and electric capability, and combined mechanical and electric drive for auxiliaries, electric clutches, and torque converters.

The architecture of an EVT-equipped HEV consists of an inner rotor connected to ICE and an outer rotor connected to the wheels through their corresponding shafts. The possibility of decoupling the wheel and engine speed can enhance the vehicle performance as the engine can operate at desired operating points [48,49]. In addition, there would be advantages of shorter maintenance intervals by preventing the mechanical losses of the gears' involvement since an electromagnetic approach can be used to split the power needless to a planetary gear system. The net power generated by the engine can partially supply the power required by the wheels while converting the remaining part to electrical form to supply the stator or be stored in the battery for propulsion [37]. In an EVT-based HEV topology, two electrical ports at the inner rotor and stator are connected to two back-to-back inverters. Figure 2 illustrates a schematic for an EVT-based passenger HEV topology.

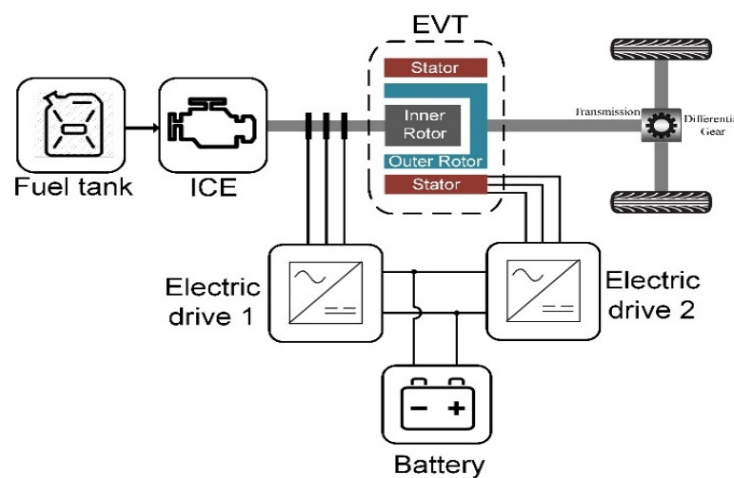


Figure 2. Hybrid electric vehicles (HEV) equipped with EVT topology.

3. Modeling and Formulation of Vehicle Subsystems

To optimize the EMS, first, it is needed to establish the vehicle's model before incorporating it in an optimization algorithm. This section goes through the modeling process of the individual components as subsystems of the vehicle model. The MATLAB/Simulink[®] version 2016b environment was used to perform the modeling, simulation, and optimization procedures in the present study. Regarding the modeling approach, the backward calculation method was employed since it combines the advantages of simplicity and low computational cost when it comes to integrating the model into the optimization procedure [37,48–50].

The required speed and acceleration time series besides the vehicle’s constant parameters (Table 1) are used in the vehicle longitudinal dynamic subsystem to calculate the tractive forces. To this end, this subsystem considers resistance forces corresponding to drag, rolling, gradient, and inertia as follows:

$$F_T = \frac{1}{2}\rho v^2 C_D A + C_r mg \cos a + mg \sin a + mC_J \frac{dv}{dt} \tag{1}$$

Table 1. Constant parameters for the vehicle dynamic calculations.

Description	Parameter (Unit)	Quantity
Drag coefficient	C_D	0.24
Rolling resistance coefficient	C_r	0.009
Rotational inertia coefficient	C_J	1.075
Frontal area	A (m ²)	1.74
Wheel radius	R_w (m)	0.287
Air Density	ρ (kg/m ³)	1.2
Auxiliary load	P (W)	500

The outputs of the vehicle dynamic subsystem are the wheels’ required torque and rotational speed, which can be readily calculated knowing the wheel’s radius:

$$T_w = F_T R_w \tag{2}$$

$$\omega_w = \frac{v}{R_w} \tag{3}$$

An input–output approach using torque–speed pairs based on the efficiency and the fuel rate maps are stored in look-up tables for the ICE subsystem. The non-scaled efficiency map of a generic ICE [37] was considered for the present study. In the fuel tank subsystem, the consumed fuel (liter) over the driving cycle can be modeled based on Equation (4), where \dot{m}_f (g/s) stands for the fuel consumption rate and ρ_f (kg/m³) represents the fuel density.

$$Fuel = \int_0^t \frac{\dot{m}_f}{\rho_f} dt \tag{4}$$

To model the battery pack, the elements of a first-order Thevenin equivalent circuit as a function of SoC were identified by using the experimental data [51] and were stored in the Simulink® look-up tables. The terminal voltage (V_{batt}) and SoC can be mathematically expressed through Equations (5)–(8), where V_{oc} is the open circuit voltage; R_{int} stands for the internal resistance; C_p and R_p represent the polarization capacitance and polarization resistance, respectively; and N_{Batt} stands for the number of the batteries. A LiFePO₄ (LFP) battery type with the specifications given in Table 2 was considered in this study.

$$I_{batt} = \frac{I_{load}}{N_{Batt}} \tag{5}$$

$$\frac{dV_{cp}}{dt} = \frac{-V_{cp}}{C_p R_p} + \frac{I_{Batt}}{C_p} \tag{6}$$

$$V_{Batt} = N_{Batts}(V_{oc} - I_{Batt}R_{int} - V_{cp}) \tag{7}$$

$$SoC = SoC_0 + \frac{1}{3600} \int \frac{I_{Batt}}{C_b} dt \tag{8}$$

Table 2. LiFePO₄ battery cell specifications.

Parameter	Quantity
Rated capacity	14 Ah
Nominal voltage	3.6 V
Max discharging current	100 A
N_{Batts}	60
$SoC_{initial}$	80%
Min Voltage	2.5
Max Voltage	4.15
C_rate charging limit	−3

Regarding the power converters, the power–efficiency pairs were stored in their corresponding look-up tables and the power flow directions were considered in the calculations. To this end, for the traction mode (while $p > 0$), the efficiency operator $\beta = -1$, and for the braking mode (while $p < 0$), the efficiency operator $\beta = 1$ are applied in Equation (9).

$$P_{out} = P_{in}\eta^\beta \tag{9}$$

The EVT subsystem consists of two concentric rotors. The inner rotor encompasses a distributed three-phase winding and the outer rotor is equipped with permanent magnets. The EVT subsystem’s inputs are the inner and the outer rotor’s torque and speed. These operating points are considered and a set of five independent currents that minimize iron and copper losses are correspondingly used in different axes (d and q). In this regard, as illustrated in Figure 3, the stator current is in the d and q -axis, the outer rotor’s current is in the d axis, and the inner rotor’s current is in the d - and q -axes [52]. Finite element (FE) calculations validated on a prototype [53] were used to store the results of the corresponding fluxes (Ψ) in look-up tables used in the EVT subsystem. Knowing the flux and current, the corresponding torque on each component can be calculated as follows, where N_p is the number of pole pairs and subscripts 1–3 are related to the stator, the outer rotor, and the inner rotor, respectively.

$$T_1 = \frac{3}{2}N_p(\psi_{1q}I_{1d} - \psi_{1d}I_{1q}) \tag{10}$$

$$T_2 = -T_1 - T_3 \tag{11}$$

$$T_3 = \frac{3}{2}N_p(\psi_{3q}I_{3d} - \psi_{3d}I_{3q}) \tag{12}$$

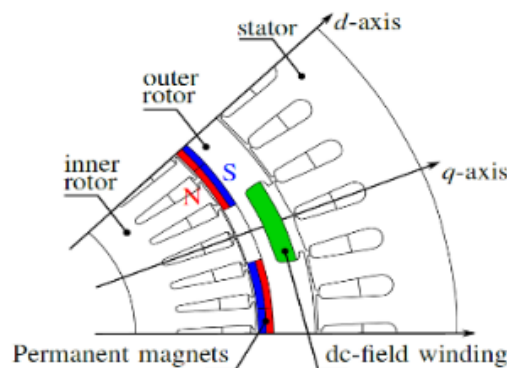


Figure 3. Cross-sectional view of the permanent magnet (PM) EVT.

The individual subsystems mathematically explained in the current section were modeled and integrated in a Simulink® environment to form the whole vehicle model, as illustrated in Figure 4.

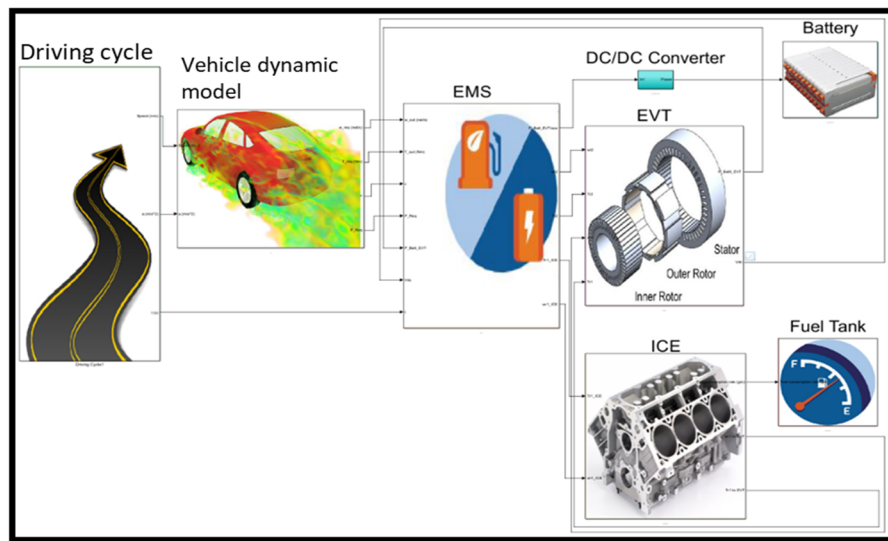


Figure 4. Diagram of the backward calculations modelled in a Simulink® environment.

4. Energy Management Strategies

The EMS block, consisting of a rule-based (RB) combined with an optimization-based (OB) approach, is the core of the power sharing control subsystem toward reaching the desired energy management objectives. The main problem of standalone RB strategies is being subjective to predefined perceptions, leading to limited objectives such as battery SoC maintenance being addressed. However, they usually end up to non-optimal solutions regarding objectives such as minimized fuel consumption. Therefore, to provide a robust EMS block, in this study, a RB-based strategy was defined and linked to OB-based strategies such as low pass filter (LPF) and ECMS for power sharing, as illustrated in Figure 5. The EMS selects operating points and modes to share the requested power between the battery and the ICE and satisfy the control objectives. The EMS must deliver the power in a way that the required driving power is fully satisfied. It operates the ICE by considering its efficiency map and charges the battery provided it is not violating the charging limitations. The SoC needs to be sustained between its intuitively and alterable defined maximum (i.e., 80%) and minimum (i.e., 75%) values, providing initial and final SoC values close enough to each other. All the objectives and their constraints need to be satisfied while minimizing the fuel consumption.

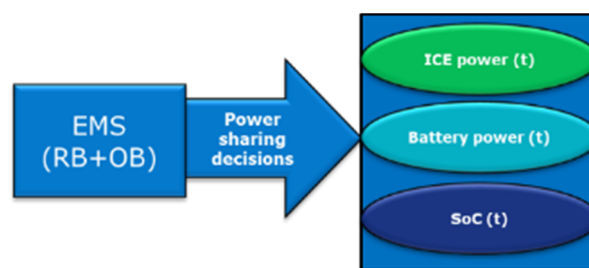


Figure 5. Power sharing based on the rule-based (RB) and optimization-based (OB) strategy.

The constraints and objectives considered for the optimization are explained in detail in the ongoing section. To recapitulate the EMS role, the considered goals are illustrated in Figure 6. The following subsections introduces the employed RB and OB strategies. The effective capability of the used EMSs in handling the goals were proven in previously performed simulation-based studies [37–39]. The present study focused on the real-time validation of the proposed strategies by performing HiL experiments in a real-time testbed. Prior to that, the next subsections will review the used RB and OB strategies in more detail.

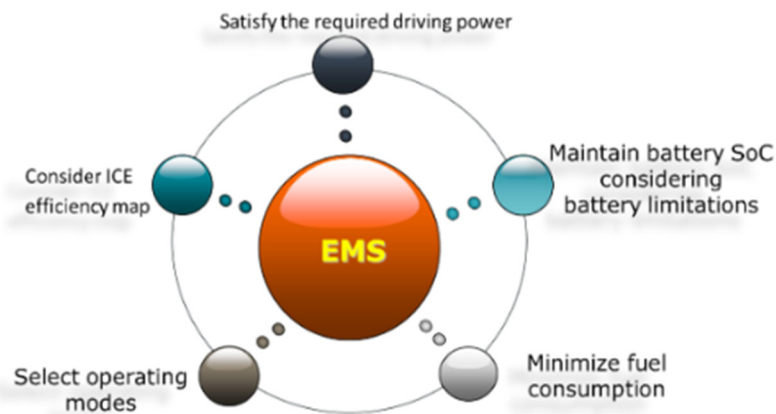


Figure 6. The energy management strategy (EMS) objectives.

4.1. Rule-Based Strategy and Operating Modes

The RB strategy considers a set of “If–Then–Else” rules based on driving patterns, SoC, and the conditions of requested versus available power. The set of desired objectives can be well-thought-of while defining these intuition-based control rules. These rules need to be included in the EMS block to work in tandem with the OB power split technique. The EMS must provide a flexible operation of the ICE in efficient operating points to meet the requested driving demands and satisfy the charging requirements. To this end, by using a speed–torque–efficiency look-up table, the EMS subsystem rules link the instantaneous split torque to its corresponding speed, leading to the highest efficiency on the engine map. The rules update the operating modes by considering the status of the demanded loads, required speeds, available energy from sources, and SoC values. The considered modes are categorized as follows.

If the requested power is greater than the available power by the ICE, it needs to be supplied in a “hybrid-traction” mode in which the required traction power will be supplied by the ICE assisted by the power drawn from the battery.

There is an opportunity to charge the battery by a part of the ICE power, if the total requested power is lower than the available ICE power. In this condition, the vehicle works in “engine-traction and battery-charging” mode in which the ICE partially supplies the requested traction power while its remaining part will charge the battery to maintain the SoC, considering its allowable minimum and maximum window range.

In the “battery-only” mode, a threshold of requested speed will be considered to turn off the ICE, and the battery pack supplies all the requested power, seeing that the battery SoC does not violate its minimum allowable value (i.e., predefined by the rules).

While braking, the battery charge can be sustained either in “hybrid battery-charging mode” or “regenerative-braking mode”, satisfying the maximum allowable SoC value. In the “hybrid battery-charging” mode, the battery is charged using the energy delivered by the ICE, aside from the energy that is partially recuperated from braking. However, in the “regenerative-braking” mode, the ICE is turned off and only the kinetic energy of braking is converted to its electrical form to supply the battery.

4.2. Low Pass Filter Power Sharing Strategy

The performance and the fuel economy of HEVs are crucial, depending on the employed power splitting methods. Hence, the utilization of a proper power splitting method in the EMS subsystem lies in the concept of power sharing between the resources toward improving the efficiency and control robustness. In this regard, an optimized low pass filter (LPF) strategy can be used by finding the proper decisive power sharing control variable (i.e., τ). The utilization of a LPF is decided on the sharing power between the supplying sources to satisfy the requested power. It uses a transfer function and

filters out the input elements and passes the output ones. To supply the demanded power, the filtered component of the power passes to be supplied by the ICE, while its difference with the total demand is supplied by the battery, taking the downstream losses into account. One should consider that the output power being delivered by the ICE needs to have enough slow variations to avoid experiencing sudden operation changes, providing an achievable actuation response. This adds to the importance of needing feasibility verifications through a HiL testbed emulating the ICE.

In the present study, a standard transfer function for the LPF was used in the energy management subsystem as follows:

$$f_{LPF} = \frac{1}{\tau \cdot s + 1} \tag{13}$$

where the control variable τ is the LPF denominator and plays the decisive power sharing role. The proper value for this control variable can be searched through an optimization routine to have the control objectives satisfied.

4.3. Equivalent Consumption Minimization Strategy (ECMS)

ECMS is a control strategy to search for an optimal power split between the ICE and battery while satisfying several equality and inequality constraints and control objectives such as SoC maintenance and fuel consumption minimization. It works based on equivalence fuel consumption factors derived as a feedback of instantaneous SoC-based functions grounded on Hamiltonian optimal control theory and Pontryagin’s minimum principle [54–57].

In ECMS, the main objective is to minimize the overall fuel consumption rate, which comprises the ICE fuel mass flow rate \dot{m}_{ICE} , plus the equivalent fuel rates of electricity \dot{m}_{eqbatt} being calculated by the equivalence factors.

$$\dot{m}_f = \dot{m}_{ICE}(t) + \dot{m}_{eqbatt}(t) \tag{14}$$

For calculation of the equivalent fuel drawn from/supplied to the battery, the equivalence factors play an important role since they directly affect the power split and consequently the fuel consumption. Optimal power sharing relies on finding the factors leading to a minimized fuel consumption. The equivalence factor K_{eqf} can be instantaneously used as a control feedback, which is a function of SoC for optimal power split and battery charge maintenance [24]. This can be expressed mathematically based on [21,58] for the formulation of the ECMS-based strategy as follows:

$$\dot{m}_{eqbatt}(t) = \frac{K_{eqf} P_{batt} \eta}{Q_{LHV}}; \text{ while charging} \tag{15}$$

$$\dot{m}_{eqbatt}(t) = \frac{K_{eqf} P_{batt}}{Q_{LHV} \eta}; \text{ while discharging} \tag{16}$$

$$K_{eqf} = \mu P_p P_I \tag{17}$$

$$x_1(t) = \frac{SoC(t) - \frac{SoC_{max} + SoC_{min}}{2}}{\frac{SoC_{max} - SoC_{min}}{2}} = \frac{2SoC(t) - (SoC_{max} + SoC_{min})}{SoC_{max} - SoC_{min}} \tag{18}$$

$$P_p(SoC) = 1 - x_1^n, \quad n = 2k + 1, \quad k \in N \tag{19}$$

$$x_2(t) = 0.01 \left(\frac{SoC_{max} + SoC_{min}}{2} - SoC(t) \right) + 0.99x_2(t - \Delta t) \tag{20}$$

$$P_I(x_2) = 1 + \tanh(nx_2) \tag{21}$$

where Q_{LHV} represents the fuel lower heating value and η is the total drivetrain chain efficiency of the downstream components included in the backward modeling. Acting as the equivalence coefficient factor, K_{eqf} is the conversion weight of the electricity into fuel. P_p and P_I are the gain multipliers controlling the stiffness and deviation of SoC around the nominal average of minimum and maximum

values. Along this line, the ECMS provides instantaneous power sharing between ICE and the battery considering predefined SoC_{min} and SoC_{max} values, current SoC values $SoC(t)$, time step Δt , and feedback gain multiplier μ as the fine-tune decision variable. To this end, ECMS updates the instantaneous equivalence factors by way of counteracting SoC deviations to maintain the SoC proportionally when it is reaching its maximum/minimum allowable values, supporting discharging/charging the battery, respectively. Figure 7 illustrates a simplified flowchart of input and output for the ECMS states.

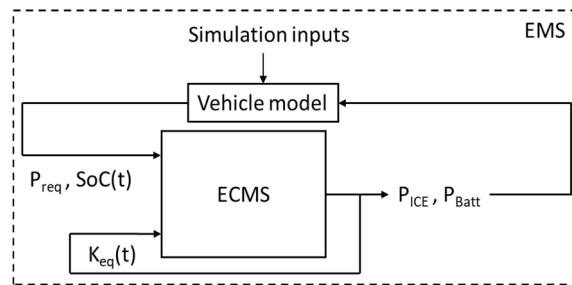


Figure 7. Simplified diagram of input and output states for ECMS.

4.4. Incorporation of the Optimization Algorithm to the Model

In this study, the decisive control parameters of the EMS cases, μ for the LPF, and τ for the ECMS, were introduced into a genetic algorithm (GA) scripted in MATLAB, which is incorporated into the Simulink-based vehicle model. The widely used GA works are based on the evolutionary process concept of natural selection in Darwin’s theory. This theory proposes that only the fittest populations can produce offspring through natural selection and survival, while unsuitable populations will be eliminated. The same concept can be conducted into mathematical optimizations where during processes like crossover, mutation, and natural selection, the good design points can be selected while neglecting worse answers toward finding optimization solutions for objective functions (survival of the fittest) [59]. The desired constraints can be defined separately or be integrated into the objective functions as penalties [16]. In the present study, the optimization algorithm and the vehicle model worked iteratively in tandem to update each other for the optimization procedure. The GA considers the decision variables as input chromosomes aside from the defined minimum and maximum values of the constraints to minimize the fuel consumption and satisfy the EMS constraints as follows.

$$\min(Fuel) = \min J = \min \int_0^t \frac{\dot{m}_f}{\rho_f} dt \tag{22}$$

$$|SoC_f - SoC_i| < \varepsilon_0 \tag{23}$$

$$SoC_{min} - \varepsilon < SoC(t) < SoC_{max} + \varepsilon \tag{24}$$

$$C_Rate(t) \geq \beta \tag{25}$$

Two sets of SoC constraints were considered here where the first one, based on Equation (23), represents the charge-maintenance requirement in HEVs. The second SoC constraint, based on Equation (24), expresses the allowable minimum and maximum limits of the SoC considered for the optimization through the driving cycle. Regarding the first mentioned inequality, the typical charge-maintaining equality $SoC_f = SoC_i$ was used to define the inequality constraint (23). Hence, ΔSoC , as the difference between the initial and final SoC values would need to stay within a small enough feasible bound ε_0 in the optimization process. It is remarkable that this constraint can be hardened/softened via altering ε_0 . Furthermore, to avoid sudden charges and to prevent fast aging of the battery pack, the EMS must consider the $C_Rate(t)$ limitation of the battery. In this regard,

the $C_Rate(t)$ constraint, based on Equation (25), of the provided features of the battery chemistry was considered where $\beta = -3$.

For the explained constraints, they were incorporated into the optimization process as penalties panelizing the objective function by adding a big enough penalty value when a desired constraint is violated. This method is a practical method to consider the constraints that cannot directly be included in the optimization formulations. The interrelations of the described modeling and optimization process are illustrated in Figure 8.

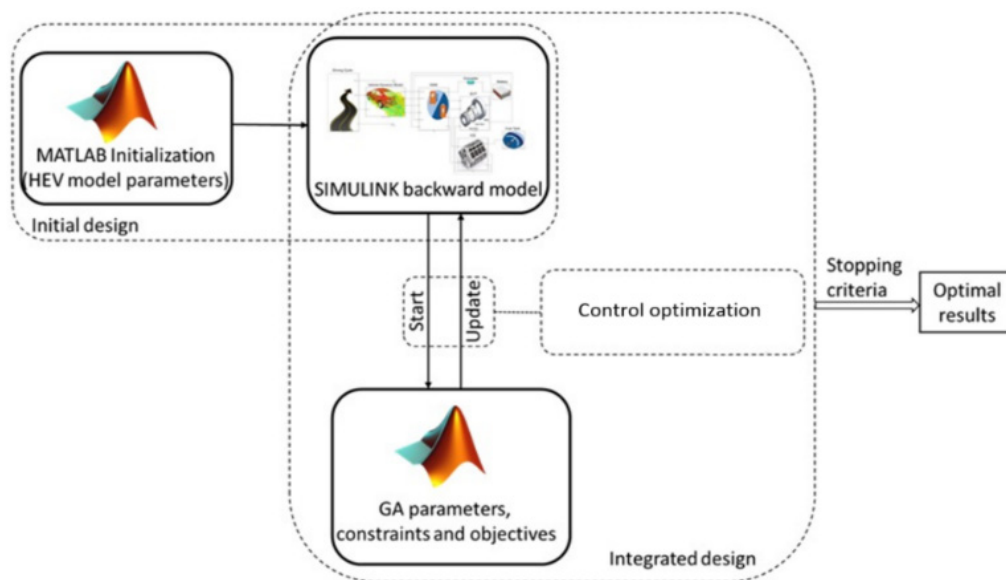


Figure 8. Coordination of the optimization algorithm and the model.

5. Case Studies and Study Procedure

This section overviews the case scenarios aside from the test procedure considered for verification purposes. Two case studies of the methodically discussed ECMS and LPF energy management approaches, each combined with the RB strategy (see Figure 9), were investigated for MiL versus HiL examinations. The cases were tested over a complete driving cycle of the New European Driving Cycle (NEDC), plotted in Figure 10, as the input of simulations and real-time implementations.

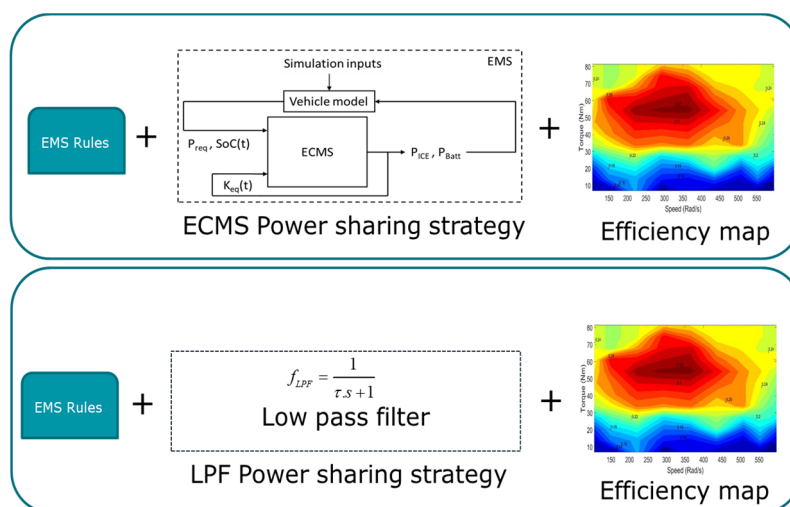


Figure 9. Overview of the considered EMS case studies, ECMS, and low pass filter (LPF) combined with RB.

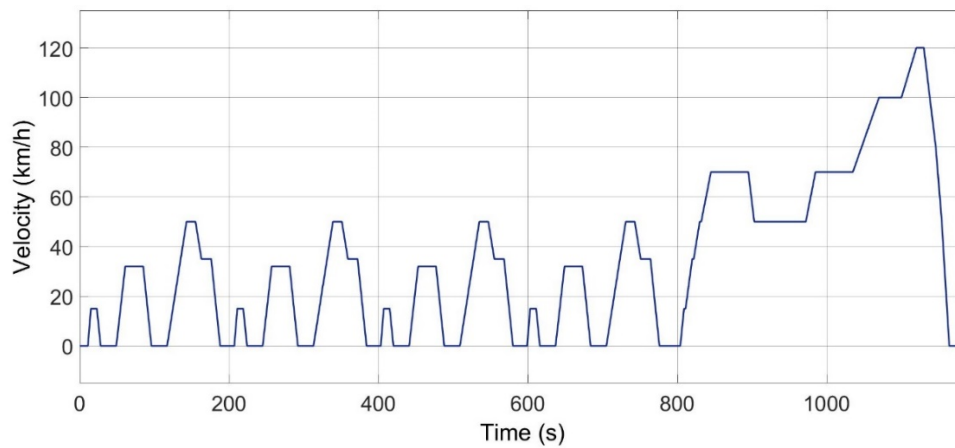


Figure 10. New European Driving Cycle (NEDC).

The study procedure consisted of different stages. First, the organized model was tested to obtain and store the results of the performed MiL simulations. Afterward, the configured EMS blocks were compiled into C Code using the Simulink[®] code generator tool and were installed into the real-time control unit of the test bench introduced in the next section. Before performing the HiL tests, pre-tests were performed using a standalone dSPACE controller to observe the EMS output signals, ensuring that the generated codes could be smoothly implemented in the main test bench. Eventually, the HiL implementation tests, each spanning 19 min and 76 s of the complete NEDC cycle, were performed and the achieved torque and speeds were stored for a comparison with those of the MiL simulations through statistical indices. In this regard, the most common engineering statistical performance indicators including root mean square error (RMSE), absolute fraction of variance (R^2), and mean square error (MSE) were applied with the outcomes of MiL simulation timeseries (X_s) and the actual experimentally measured HiL timeseries (X_a) to analyze and verify the performance of the real-time implementation. RMSE provides error information on short-term performance, as it allows a term-by-term comparison of the actual deviation between the simulated and the measured values [60]. Hence, low RMSE and MSE values are generally favorable. The very commonly used agreement coefficient R^2 is a measure indicating the relationship between values under comparison as a function of RMSE and standard deviation. To compare the two datasets, the standard deviation was constant, so clearly, the R^2 values were expected to increase with degradation of RMSEs. Table 3 provides the utilized statistical indicators accompanied by their mathematical expressions, and Figure 11 depicts a diagram of the study procedure.

Table 3. Statistical performance indices.

Performance Index	Expression
RMSE	$\sqrt{\frac{1}{n} \sum_{i=1}^n (X_{i,s} - X_{i,a})^2}$
R^2	$\frac{\sum_{i=1}^n (X_{i,s} - X_{s,avg}) \times (X_{i,a} - X_{a,avg})}{\sqrt{\left[\sum_{i=1}^n (X_{i,s} - X_{i,s})^2 \right] \times \left[\sum_{i=1}^n (X_{i,a} - X_{a,avg})^2 \right]}}$
MSE	$\frac{1}{n} \sum_{i=1}^n (X_{i,s} - X_{i,a})^2$

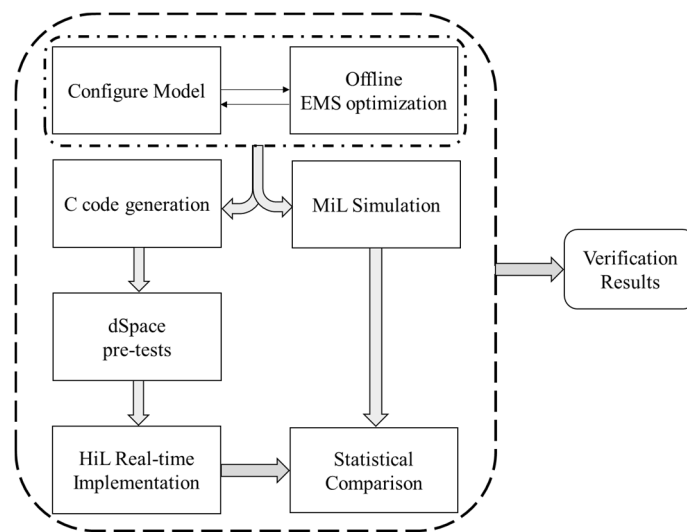


Figure 11. Study procedure of hardware-in-the-loop (HiL) vs. model-in-the-loop (MiL) verification.

6. Hardware-in-the-Loop (HiL) Testbed Structure and Specifications

The testbed components are actuated based on decisions made by the optimized EMS control besides the EVT local control units while considering the emulated torque and speed corresponding to the input driving profile. To this end, C codes generated from the optimized EMS blocks are uploaded to the control unit of the lab testbed for separated cases. The local control of the EVT machine worked based on the previously discussed set of currents applied to the machine. These currents are controlled using two inverters, and a current regulated dc-power supply. The sensing, measuring, and the control units send/receive the dataset and corresponding commands to/from mechanical and electrical components and their linkages are illustrated in Figure 12.

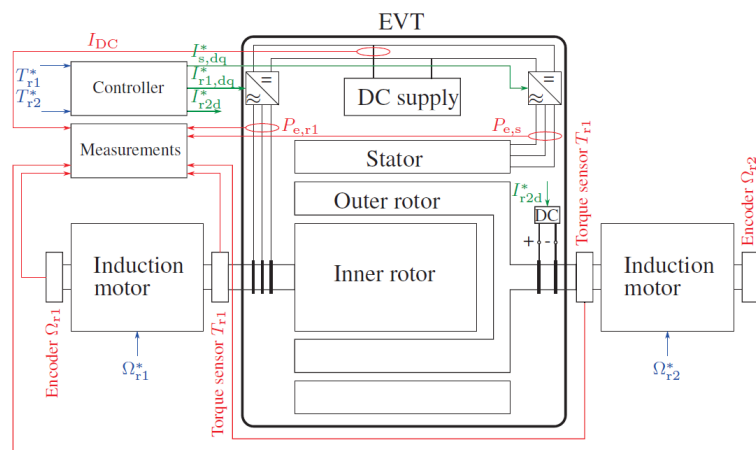


Figure 12. Schematic of the experimental setup [61].

Figure 13 presents a panorama of the laboratory experimental setup used for the real-time implementation. The EVT machine with 120 kW rated power was placed in the middle and coupled to two 30 kW induction motors located at the left (connected to inner rotor) and right (connected to outer rotor) sides. The two electrical ports at the inner rotor and stator were connected to two water cooled 150 kW and 100 kW inverters, respectively.

In the prepared testbed, the left induction motor was controlled to represent an ICE and was connected to the inner rotor of the EVT. Compared to conventional setups, replacing an induction motor for a real engine in the testbed produced the following advantages:

- A real engine produces tail gas during the test and causes pollution in contrast to an induction machine.
- To test a different design, an engine must be replaced with another specific one, whereas using the induction machine can provide more flexibility in terms of scaling.
- Operating an engine in the test environment comes with lower safety and higher operating costs when compared to an induction motor.

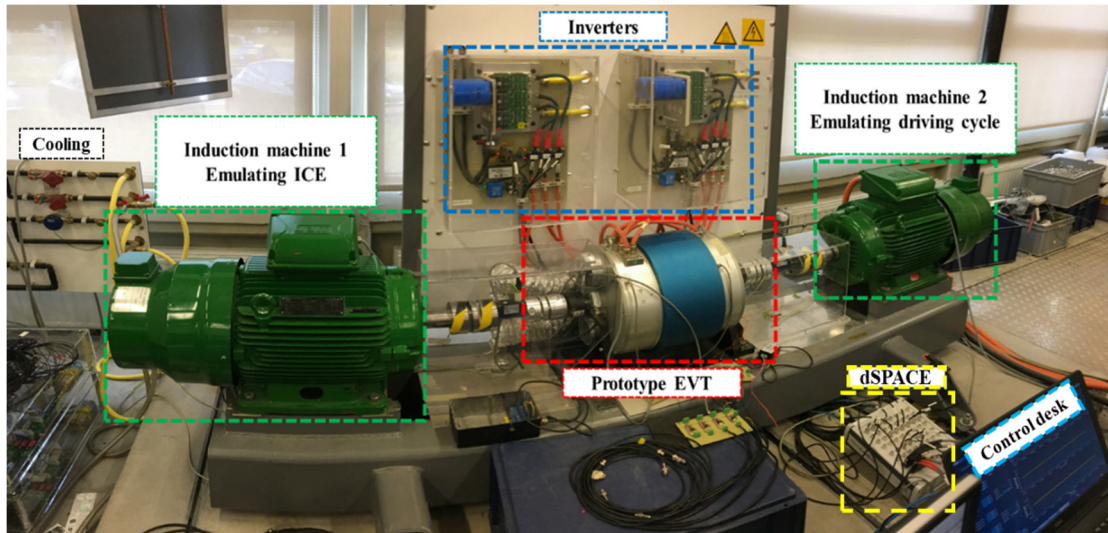


Figure 13. Experimental test bench of the study.

On the right-hand, a second induction motor was connected to the outer rotor to emulate the road profile input based on the NEDC. The battery was replaced by a 40-kW dc power supply in the test bench. Torque sensors (with a maximum measurable torque of 100 Nm) and encoders were used to measure the torque and rotational speed of the inner and outer rotors, respectively, and the electrical power flows were measured by using a power analyzer. It is noteworthy that the measuring limitation of the setup’s torque sensors ($T < 100\text{ N}$), maximum speed limitation of the inner rotor ($\Omega r1 < 4300\text{ rpm}$), maximum speed limitation of the outer rotor ($\Omega r2 < 4300\text{ rpm}$), and a setup safety shutdown limitation, related to the difference between the inner and outer rotor speeds ($|\Omega r1 - \Omega r2| < 4000$), were already considered in the optimized blocks uploaded to the control units. The dSPACE MicroLabBox was used with a fixed time step of $TS = 0.0001\text{ s}$ for the components’ local control and $TS = 1$ for the EMS to ensure adequate data resolution. Table 4 represents the specifications of the setup parameters in more detail, and Figure 14 plots the demand power of the cycle considered for the examinations.

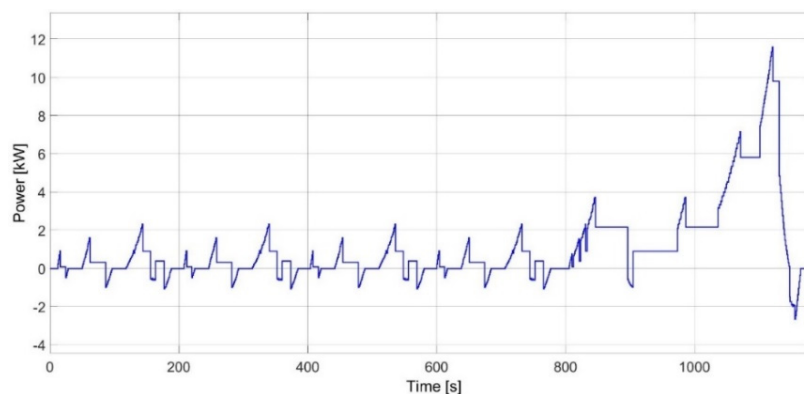


Figure 14. Demand load considered for the examinations.

Table 4. Prototype machine parameters.

Parameter	Stator	Outer Rotor	Inner Rotor
Rated mechanical power [kW]	-	120	75
Rated current amplitude [A]	265	4.6 (dc)	150
Max speed [r/min]	-	6000	6000
Torque sensor limitation (Nm)	-	100	100
Continuous torque [Nm]	245	382	137
Number of slots N	48	-	48
Number of pole pairs Np	4	4	4
Outer radius [mm]	175	123.5	102
Inner radius [mm]	124.5	103	57
PM thickness [mm]	-	5	-
Active axial length l_{ax} [mm]	87	87	87
Number of slots	48	8	48
Number of slots per pole and per phase	2	1	2
Number of windings in series per phase and per pole pare	12	240	10

7. Results and Discussion

After performing the HiL implementations over the NEDC, real-time results for the inner and outer rotor actuations including the torque and speed dataset were achieved and stored. These results were compared with the corresponding ones acquired from the MiL simulations. The MiL vs. HiL results were plotted to observe the response performances and agreement accuracies for the studied cases. Accordingly, the statistical performance indices were applied over those dataset pairs, and calculated results are provided for long-term verification as follows.

For the LPF-based EMS case, Figure 15 illustrates the results of the outer rotor torques. The speed results for the same rotor are plotted in Figure 16. With regard to the inner rotor, the achieved speed and torque results of the same case are presented in Figures 17 and 18, respectively. Figure 19 illustrates the obtained SoC for this case. For the ECMS-based case study, Figure 20 illustrates the results for the outer rotor torques, while the speed results for the same rotor are plotted in Figure 21. Consequently, the speed and torque results of the inner rotor for this case are presented in Figures 22 and 23, respectively. Figure 24 illustrates the obtained SoC for this case. Considering Figures 15–18, Figures 20–23, an investigation of the results through the cycle indicates that the actual torque and speed values obtained from the HiL implementations could closely follow the MiL simulations with well-matched responses for both of the studied EMSs. Along the same line, Figure 25 provides the error histogram for the investigated MiL vs. HiL occurrences where normal distributions around zero error values were favorably observed. The allowable SoC range considered 75% for the minimum and 80% for the maximum thresholds. As can be seen in Figures 19 and 24, both employed strategies could well-maintain the SoC by achieving close enough initial and final values as desired. Regarding the MiL vs. HiL results, some inevitable mismatches related to noises were observed. These inevitable deviations could be expected, as has also been widely observed in the results of similar studies performed previously such as in [8,25,26,62]. This can be interpreted as mismeasurements imposed on the sensors by the laboratory's environmental conditions, machine vibrations, or abrupt accelerations of the induction machines. Regarding the minor noises, they can be more readily recognized where the measured HiL data exhibited values slightly greater/smaller than zero whereas the MiL dataset appropriately followed zero values for the same instants. From what was physically observed in the lab through multiple similar examinations, there were no rotational actuations for those moments in the HiL tests, making them indeed comply with the MiL results. Hence, for the mismeasurements, it can be seen that vibrations coming from a rotating rotor (e.g., outer) would slightly affect the measuring quality of a standstill rotor's sensor (e.g., inner). Furthermore, noises from the lab environment, the testing conditions, and the air quality (e.g., dust, temperature, humidity, etc.) might cause these types of inevitable noises to be recorded. On the other hand, other mismatches were observed where

the actuations started undertaking great changes. As expected, when sudden accelerations were imposed by either of the two induction machines (e.g., see Figure 15, $t = 200$ s), the measuring quality was affected by exhibiting an overshoot for a short instant (inertia effect).

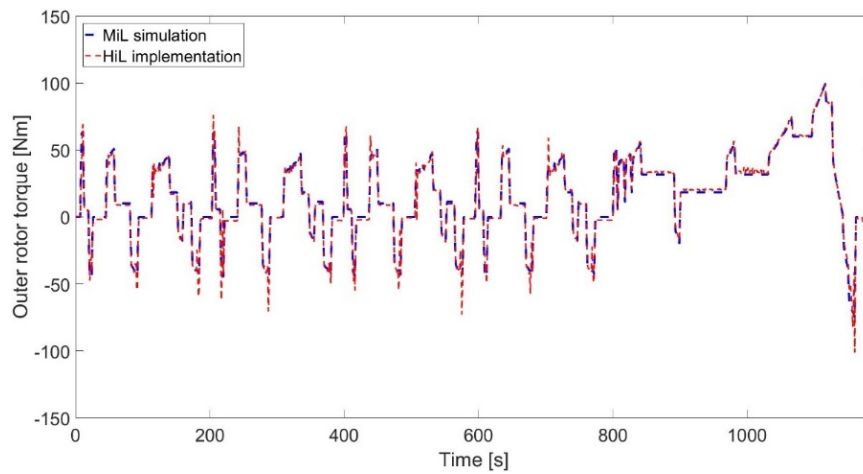


Figure 15. HiL (experimental) vs. MiL agreement results for the outer rotor torque, LPF-based EMS.

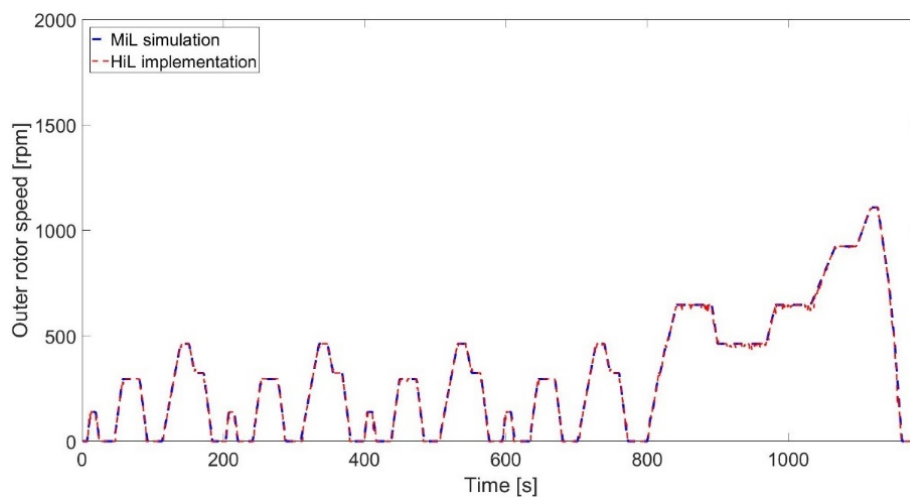


Figure 16. HiL (experimental) vs. MiL agreement results for the outer rotor speed, LPF-based EMS.

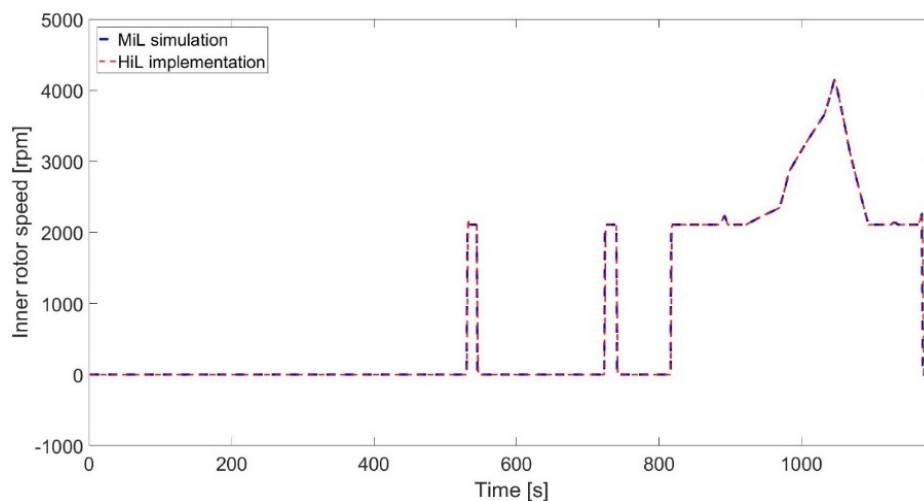


Figure 17. HiL (experimental) vs. MiL agreement results for the inner rotor speed, LPF-based EMS.

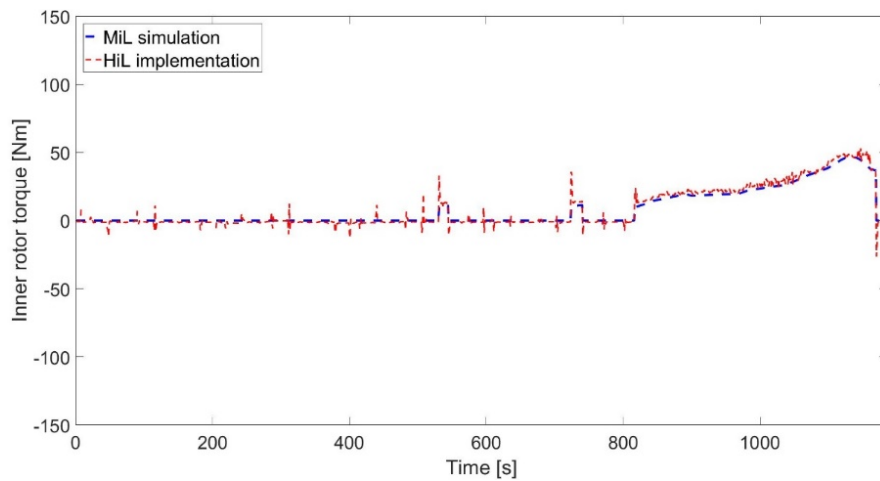


Figure 18. HiL (experimental) vs. MiL agreement results for the inner rotor torque, LPF-based EMS.

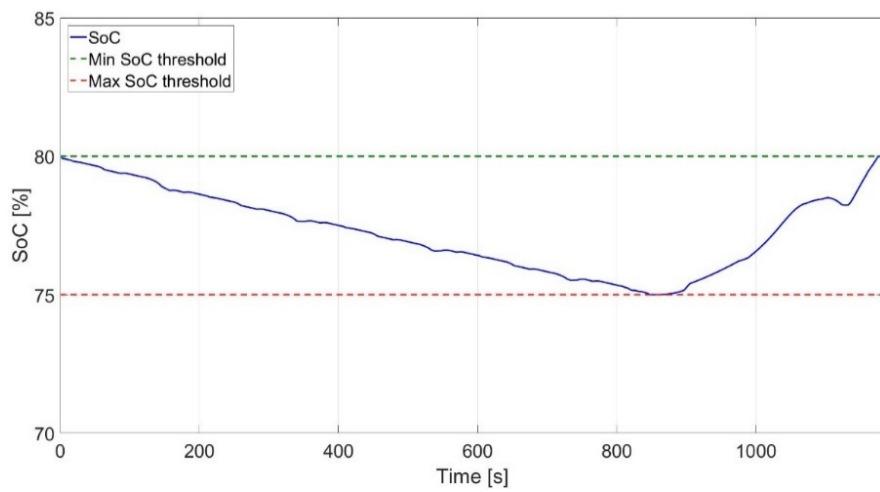


Figure 19. SoC trend, LPF-based EMS.

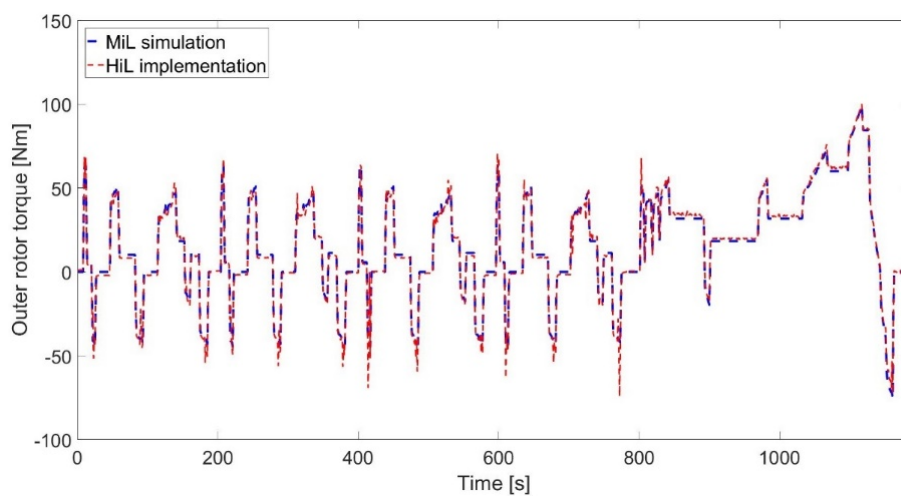


Figure 20. HiL (experimental) vs. MiL agreement results for the outer rotor torque, ECMS-based EMS.

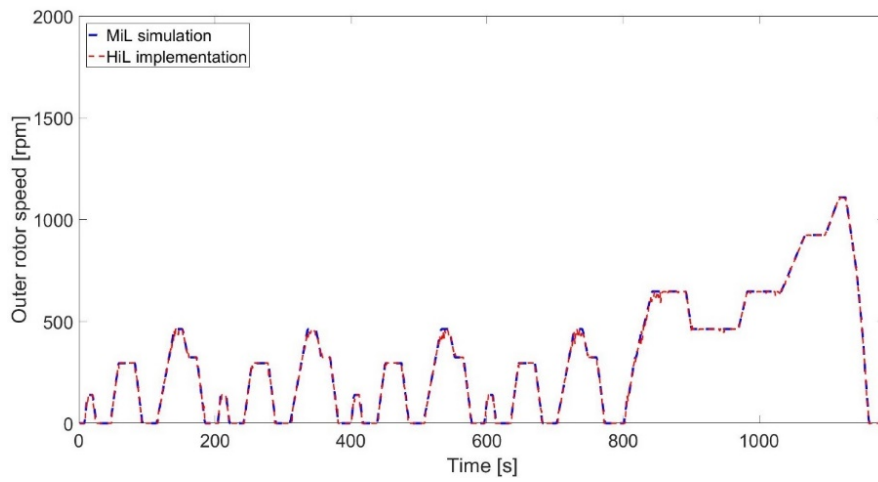


Figure 21. HiL (experimental) vs. MiL agreement results for the outer rotor speed, ECMS-based EMS.

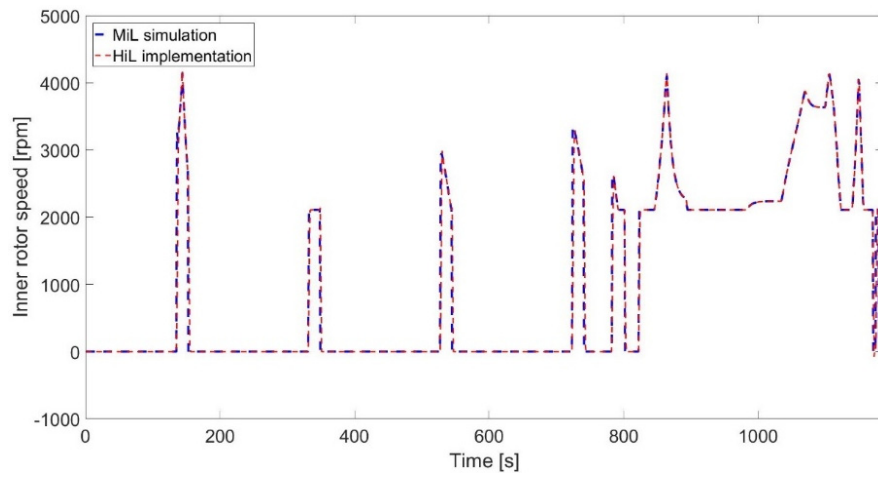


Figure 22. HiL (experimental) vs. MiL agreement results for the inner rotor speed, ECMS-based EMS.

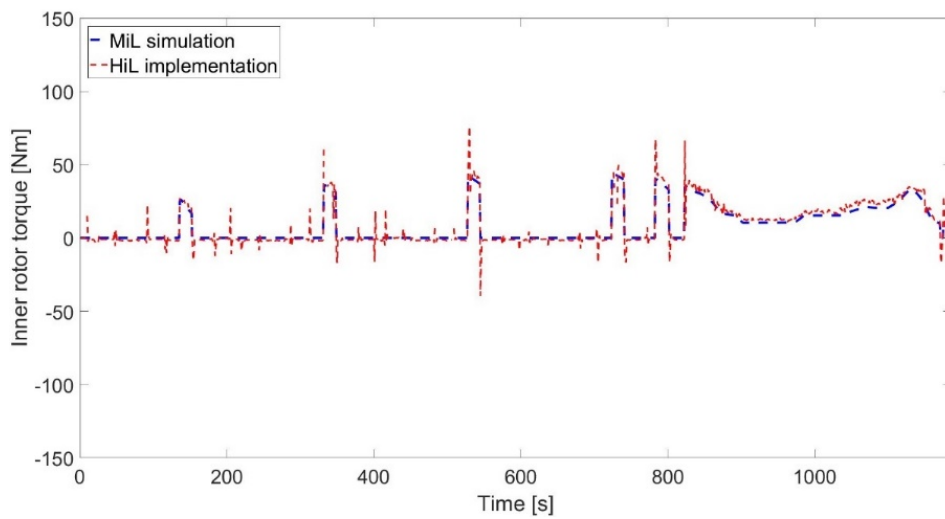


Figure 23. HiL (experimental) vs. MiL agreement results for the inner rotor torque, ECMS-based EMS.

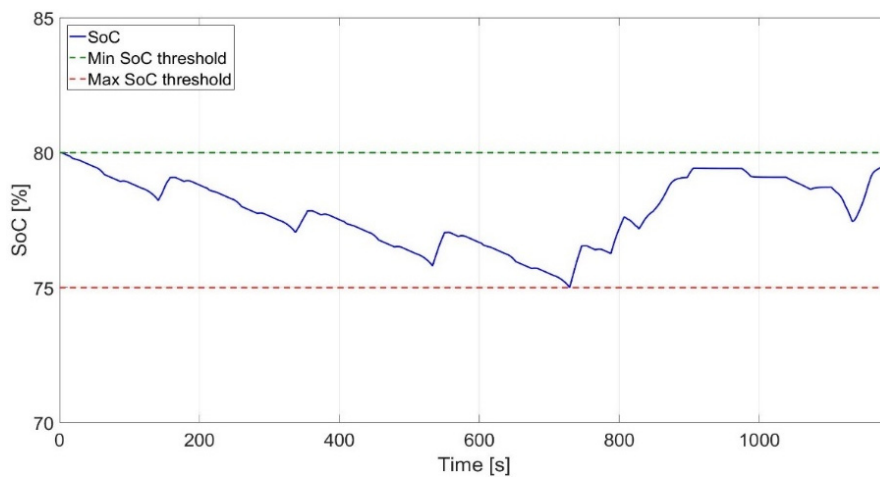


Figure 24. SoC trend, ECMS-based EMS.

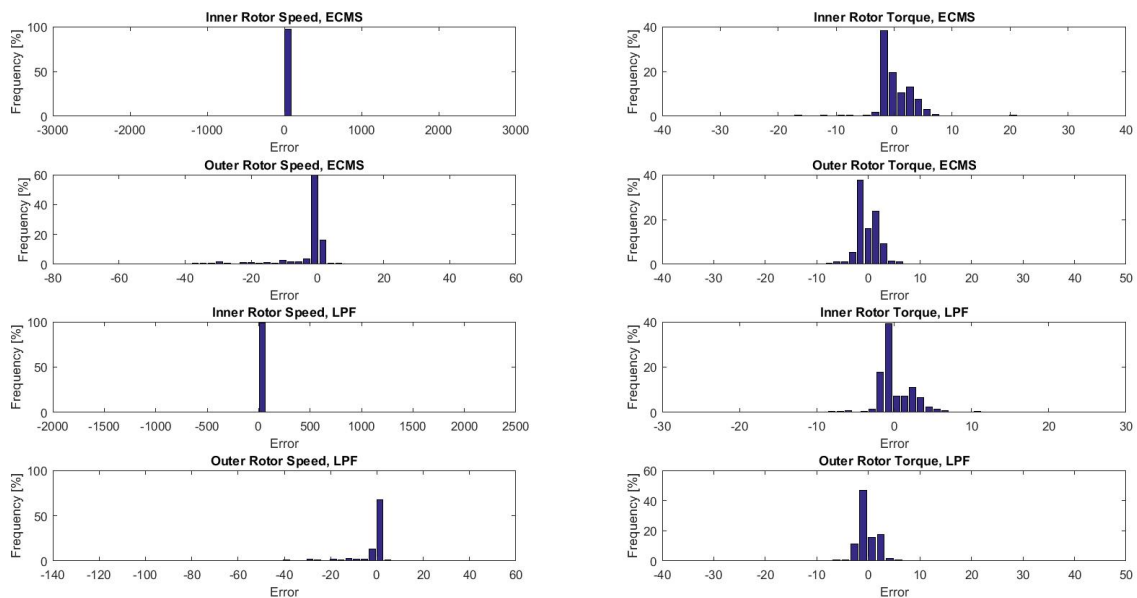


Figure 25. HiL vs. MiL error histograms.

For a precise performance evaluation, long-term statistical analyses of the obtained results considering the whole cycle is necessary. Hence, the previously introduced statistical performance indices were applied over the obtained MiL vs. HiL results and the calculation outcomes for the studied cases are provided in Tables 5 and 6. Although the discussed measuring mismatches were seen in the calculations, quite favorable values were achieved for RMSE and MSE (both close to 0) and R^2 (close to 1), knowing the minimum and maximum ranges of the compared datasets. This indicates the fast and accurate response capability of the tested EMSs in such a real-time application and was validated using the prepared test bench. The versatile testbed provided for the studied topology can be used for similar studies to test the applicability of other combined/standalone EMS types and validate their HiL vs. MiL/SiL results, paving the way toward vehicle-in-the-loop experiments.

Table 5. Statistical performance analysis results, LPF-based case study.

	Outer Rotor		Inner Rotor	
	Torque	Speed	Torque	Speed
R ²	0.98	0.99	0.98	0.99
RMSE	0.15	0.03	0.24	0.07
MSE	0.02	0.001	0.05	0.006

Table 6. Statistical performance analysis results, ECMS-based case study.

	Outer Rotor		Inner Rotor	
	Torque	Speed	Torque	Speed
R ²	0.99	0.99	0.80	0.98
RMSE	0.12	0.03	0.91	0.18
MSE	0.01	0.001	0.84	0.03

8. Conclusions and Future Work Directions

This paper reported the HiL vs. MiL evaluations for two proposed power split strategies intended for a recent topology of passenger vehicles, HEVs equipped with EVT. First, a detailed vehicle model was built at the component level and linked to the provided optimized EMSs in a MATLAB/Simulink[®] environment to obtain the MiL simulation results. Next, a versatile test bench representing the vehicle architecture was prepared in the presence of physical components. Two of the studied control strategies were uploaded into the controller hardware unit and the real-time HiL implementations results for a full driving cycle were achieved. Upon successful HiL and MiL tests over the cycle, the paper performed comparative analyses by applying different statistical agreement and error evaluation indices. The investigation of the results for both studied EMSs indicated that the torque and speed actuation results obtained from the HiL implementations could closely comply with the MiL ones. The evaluations validated the implementation ability of the studied cases with robust accuracy and fast actuation response in such a real-time environment.

Knowing the driving cycle trends in advance, offline EMSs were tested in this study. Future work directions can include evaluation of online strategies using the provided testbed. Furthermore, investigation of different control strategies linked to the component' optimal sizing concept merits as a future subject matter paving the design way toward vehicle-in-the-loop experiments and validation studies for real-world applications.

Author Contributions: Conceptualization, M.V. and O.H.; Methodology, M.V.; Software, M.V. and F.V.; Validation, M.V.; Formal analysis, M.V.; Investigation, M.V.; Writing—Original draft preparation, M.V.; Writing—Review and editing, M.V., O.H., M.E.B., and F.V.; Visualization, M.V. and F.V.; Supervision, O.H., P.S., and J.V.M. All authors have read and agreed to the published version of the manuscript.

Funding: This research received no external funding.

Acknowledgments: The authors are grateful to VLAIO (ex. IWT) and Flanders Make, national funding schemes in Belgium, for their support to the current work, performed within the EMTechno project (project ID: IWT150513).

Conflicts of Interest: The authors declare no conflicts of interest.

Abbreviations

EMS	Energy Management Strategy
CAN	Controller Area Network
DSP	Digital Signal Processing
EVT	Electrical Variable Transmission
ECMS	Equivalent Consumption Minimization Strategy
FE	Finite element
FC	Fuel Cell
GA	Genetic Algorithm
HiL	Hardware-in-the-Loop
HEV	Hybrid Electric Vehicle
ICE	Internal Combustion Engine
LFP	LiFePO ₄
LPF	Low Pass Filter
MSE	Mean Square Error
MiL	Model-in-the-Loop
NEDC	New European Driving Cycle
OB	Optimization-Based
PMS	Power Management Strategy
PM	Permanent Magnet
PiL	Processor-in-the-Loop
RTI	Real-time Interface
RTW	Real-Time workshop
RMSE	Root Mean Square Error
RB	Rule-Based
SiL	Software-in-the-Loop
SC	Super Capacitor
SoC	State of Charge
ViL	Vehicle-in-the-Loop

References

1. Fazelpour, F.; Vafaeipour, M.; Rahbari, O.; Rosen, M.A. Intelligent optimization of charge allocation for plug-in hybrid electric vehicles utilizing renewable energy considering grid characteristics. In Proceedings of the IEEE International Conference on Smart Energy Grid Engineering, Oshawa, ON, Canada, 28–30 August 2013; pp. 1–8.
2. Fazelpour, F.; Vafaeipour, M.; Rahbari, O.; Rosen, M.A. Intelligent optimization to integrate a plug-in hybrid electric vehicle smart parking lot with renewable energy resources and enhance grid characteristics. *Energy Convers. Manag.* **2014**, *77*, 250–261. [[CrossRef](#)]
3. Rahbari, O.; Vafaeipour, M.; Omar, N.; Rosen, M.A.; Hegazy, O.; Timmermans, J.-M.; Heibati, S.; Van Den Bossche, P. An optimal versatile control approach for plug-in electric vehicles to integrate renewable energy sources and smart grids. *Energy* **2017**, *134*, 1053–1067. [[CrossRef](#)]
4. Nagaraj, S.C.; Detrick, B. HIL and RCP tools for embedded controller development in hybrid vehicles. In Proceedings of the IEEE Vehicle Power and Propulsion Conference, Dearborn, MI, USA, 7–11 September 2009; pp. 896–902.
5. Li, Y.; Agashe, P.; Ge, Z.; Chen, B. Rapid prototyping energy management system for a single shaft parallel hybrid electric vehicle using hardware-in-the-loop simulation. *SAE Int. J. Altern. Powertrains* **2013**, *2*, 241–251. [[CrossRef](#)]
6. Zhao, H.; Cheng, L.; Zhang, G. Design of a versatile test bench for hybrid electric vehicles. In Proceedings of the IEEE Vehicle Power and Propulsion Conference, Harbin, China, 3–5 September 2008; pp. 1–4.
7. Garousi, V.; Felderer, M.; Karapıçak, Ç.M.; Yılmaz, U. Testing embedded software: A survey of the literature. *Inf. Softw. Technol.* **2018**, *104*, 14–45. [[CrossRef](#)]
8. Yang, C.; Du, S.; Li, L.; You, S.; Yang, Y.; Zhao, Y. Adaptive real-time optimal energy management strategy based on equivalent factors optimization for plug-in hybrid electric vehicle. *Appl. Energy* **2017**, *203*, 883–896. [[CrossRef](#)]

9. Wei, Z.; Xu, J.; Halim, D. HEV power management control strategy for urban driving. *Appl. Energy* **2017**, *194*, 705–714. [[CrossRef](#)]
10. Peng, J.; He, H.; Xiong, R. Rule based energy management strategy for a series–parallel plug-in hybrid electric bus optimized by dynamic programming. *Appl. Energy* **2017**, *185*, 1633–1643. [[CrossRef](#)]
11. Venditti, M. Analysis of the performance of different machine learning techniques for the definition of rule-based control strategies in a parallel HEV. *Energy Procedia* **2016**, *101*, 685–692. [[CrossRef](#)]
12. Wu, J.; Peng, J.; He, H.; Luo, J. Comparative analysis on the rule-based control strategy of two typical hybrid electric vehicle powertrain. *Energy Procedia* **2016**, *104*, 384–389. [[CrossRef](#)]
13. Neffati, A.; Caux, S.; Fadel, M. Fuzzy switching of fuzzy rules for energy management in HEV. *IFAC Proc. Vol.* **2012**, *45*, 663–668. [[CrossRef](#)]
14. Wei, Z.; Xu, Z.; Halim, D. Study of HEV power management control strategy based on driving pattern recognition. *Energy Procedia* **2016**, *88*, 847–853. [[CrossRef](#)]
15. Huang, Y.-J.; Yin, C.-L.; Zhang, J.-W. Design of an energy management strategy for parallel hybrid electric vehicles using a logic threshold and instantaneous optimization method. *Int. J. Automot. Technol.* **2009**, *10*, 513–521. [[CrossRef](#)]
16. Montazeri-Gh, M.; Poursamad, A. Application of genetic algorithm for simultaneous optimisation of HEV component sizing and control strategy. *Int. J. Altern. Propuls.* **2006**, *1*, 63–78.
17. Gao, W.; Porandla, S.K. Design optimization of a parallel hybrid electric powertrain. In Proceedings of the IEEE Vehicle Power and Propulsion Conference, Chicago, IL, USA, 7 September 2005; p. 6.
18. Salmasi, F.R. Control strategies for hybrid electric vehicles: Evolution, classification, comparison, and future trends. *IEEE Trans. Veh. Technol.* **2007**, *56*, 2393–2404. [[CrossRef](#)]
19. Martinez, C.M.; Hu, X.; Cao, D.; Velenis, E.; Gao, B.; Wellers, M. Energy management in plug-in hybrid electric vehicles: Recent progress and a connected vehicles perspective. *IEEE Trans. Veh. Technol.* **2016**, *66*, 4534–4549. [[CrossRef](#)]
20. Musardo, C.; Rizzoni, G.; Guezennec, Y.; Staccia, B. A-ECMS: An adaptive algorithm for hybrid electric vehicle energy management. *Eur. J. Control* **2005**, *11*, 509–524. [[CrossRef](#)]
21. Gu, B.; Rizzoni, G. An adaptive algorithm for hybrid electric vehicle energy management based on driving pattern recognition. In Proceedings of the ASME International Mechanical Engineering Congress and Exposition, Chicago, IL, USA, 5–10 November 2006; pp. 249–258.
22. Chasse, A.; Sciarretta, A.; Chauvin, J. Online optimal control of a parallel hybrid with costate adaptation rule. *IFAC Proc. Vol.* **2010**, *43*, 99–104. [[CrossRef](#)]
23. Kessels, J.T.; Koot, M.W.; Van Den Bosch, P.P.; Kok, D.B. Online energy management for hybrid electric vehicles. *IEEE Trans. Veh. Technol.* **2008**, *57*, 3428–3440. [[CrossRef](#)]
24. Onori, S.; Serrao, L.; Rizzoni, G. Adaptive equivalent consumption minimization strategy for hybrid electric vehicles. In Proceedings of the ASME Dynamic Systems and Control Conference, Cambridge, MA, USA, 13–15 September 2010; pp. 499–505.
25. Schupbach, R.M.; Balda, J.C. A versatile laboratory test bench for developing powertrains of electric vehicles. In Proceedings of the IEEE 56th Vehicular Technology Conference, Vancouver, BC, Canada, 24–28 September 2002; pp. 1666–1670.
26. Moulik, B.; Söffker, D. Online power management with embedded offline-optimized parameters for a three-source hybrid powertrain with an experimental emulation application. *Energies* **2016**, *9*, 439. [[CrossRef](#)]
27. Wu, H.; Zhang, H.; Motevalli, V.; Qian, Y.; Wolfe, A. Hybrid Electric Vehicle Powertrain Controller Development Using Hardware in the Loop Simulation. SAE Technical Paper. Available online: https://www.researchgate.net/publication/270686871_Hybrid_Electric_Vehicle_Powertrain_Controller_Development_Using_Hardware_in_the_Loop_Simulation (accessed on 8 April 2013).
28. Wang, L.; Zhang, Y.; Yin, C.; Zhang, H.; Wang, C. Hardware-in-the-loop simulation for the design and verification of the control system of a series–parallel hybrid electric city-bus. *Simul. Model. Pract. Theory* **2012**, *25*, 148–162. [[CrossRef](#)]
29. Algarny, K.; Abdelrahman, A.S.; Youssef, M. A novel platform for power train model of electric cars with experimental validation using real-time hardware in-the-loop (HIL): A case study of GM Chevrolet Volt 2nd generation. In Proceedings of the IEEE Applied Power Electronics Conference and Exposition (APEC), San Antonio, TX, USA, 4–8 March 2018; pp. 3510–3516.

30. Chacko, R.V.; Sreedevi, M.; Mineeshma, G. Electric vehicle power train simulation in forward modelling approach to enable real-time simulation and HIL controller prototyping. In Proceedings of the IEEE International Conference on Power Electronics, Drives and Energy Systems (PEDES), Mumbai, India, 16–19 December 2014; pp. 1–6.
31. Nair, V.V.; Pathiyil, P. High dynamic HIL model for complete software testing solution of Hev/Ev. In Proceedings of the IEEE International Transportation Electrification Conference (ITEC), Chennai, India, 27–29 August 2015; pp. 1–7.
32. Mayyas, A.R.O.; Kumar, S.; Pisu, P.; Rios, J.; Jethani, P. Model-based design validation for advanced energy management strategies for electrified hybrid power trains using innovative vehicle hardware in the loop (VHIL) approach. *Appl. Energy* **2017**, *204*, 287–302. [[CrossRef](#)]
33. Chasse, A.; Sciarretta, A. Supervisory control of hybrid powertrains: An experimental benchmark of offline optimization and online energy management. *Control Eng. Pract.* **2011**, *19*, 1253–1265. [[CrossRef](#)]
34. Castaings, A.; Bouscayrol, A.; Lhomme, W.; Trigui, R. Power hardware-in-the-loop simulation for testing multi-source vehicles. *IFAC PapersOnLine* **2017**, *50*, 10971–10976. [[CrossRef](#)]
35. Castaings, A.; Lhomme, W.; Trigui, R.; Bouscayrol, A. Comparison of energy management strategies of a battery/supercapacitors system for electric vehicle under real-time constraints. *Appl. Energy* **2016**, *163*, 190–200. [[CrossRef](#)]
36. Allègre, A.-L.; Bouscayrol, A.; Trigui, R. Flexible real-time control of a hybrid energy storage system for electric vehicles. *IET Electr. Syst. Transp.* **2013**, *3*, 79–85. [[CrossRef](#)]
37. Vafaeipour, M.; El Baghdadi, M.; Verbelen, F.; Sergeant, P.; Van Mierlo, J.; Stockman, K.; Hegazy, O. Technical assessment of utilizing an electrical variable transmission system in hybrid electric vehicles. In Proceedings of the IEEE Transportation Electrification Conference and Expo, Asia-Pacific (ITEC Asia-Pacific), Bangkok, Thailand, 6–9 June 2018; pp. 1–5.
38. Vafaeipour, M.; El Baghdadi, M.; Van Mierlo, J.; Hegazy, O.; Verbelen, F.; Sergeant, P. An ECMS-based approach for energy management of a HEV equipped with an electrical variable transmission. In Proceedings of the Fourteenth International Conference on Ecological Vehicles and Renewable Energies (EVER), Monte-Carlo, Monaco, 8–10 May 2019; pp. 1–9.
39. Vafaeipour, M.; Tran, D.-D.; El Baghdadi, M.; Verbelen, F.; Sergeant, P.; Stockman, K.; Van Mierlo, J.; Hegazy, O. Optimized energy management strategy for a HEV equipped with an electrical variable transmission system. In Proceedings of the 32nd Electric Vehicle Symposium (EVS32), Lyon, France, 19–22 May 2019.
40. Cheng, Y.; Espanet, C.; Trigui, R.; Bouscayrol, A.; Cui, S. Design of a permanent magnet electric variable transmission for HEV applications. In Proceedings of the IEEE Vehicle Power and Propulsion Conference, Lille, France, 1–3 September 2010; pp. 1–5.
41. Nordlund, E.; Eriksson, S. Test and verification of a four-quadrant transducer for HEV applications. In Proceedings of the IEEE Vehicle Power and Propulsion Conference, Chicago, IL, USA, 7–9 September 2005; p. 5.
42. Pisek, P.; Stumberger, B.; Marcic, T.; Virtic, P. Design analysis and experimental validation of a double rotor synchronous PM machine used for HEV. *IEEE Trans. Magn.* **2012**, *49*, 152–155. [[CrossRef](#)]
43. Verbelen, F.; Vansompel, H.; Abdallah, A.; Stockman, K.; Sergeant, P. Design methodology for a PM electrical variable transmission used in HEV. In Proceedings of the EEMODS, Tokyo, Japan, 17–19 September 2019.
44. Li, Z.; Ma, Z.; Cui, S. Design of hardware-in-the-loop simulation platform for Electric Variable Transmission (EVT) based HEV power train. In Proceedings of the IEEE Conference and Expo Transportation Electrification Asia-Pacific (ITEC Asia-Pacific), Beijing, China, 31 August–3 September 2014; pp. 1–6.
45. Li, Z.; Ma, Z.; Cui, S. Design and research on engine emulation system of HEV power train hardware-in-the-loop simulation platform. In Proceedings of the IEEE Conference and Expo Transportation Electrification Asia-Pacific (ITEC Asia-Pacific), Beijing, China, 31 August–3 September 2014; pp. 1–6.
46. Hoeijmakers, M.J. Rotating Electromechanical Converter. U.S. Patent 9,018,863, 28 April 2015.
47. Hoeijmakers, M.J.; Ferreira, J.A. The electric variable transmission. *IEEE Trans. Ind. Appl.* **2006**, *42*, 1092–1100. [[CrossRef](#)]
48. Chehresaz, M. *Modeling and Design Optimization of Plug-In Hybrid Electric Vehicle Powertrains*; University of Waterloo: Waterloo, ON, Canada, 2013.
49. Millo, F.; Rolando, L.; Andreatta, M. Numerical simulation for vehicle powertrain development. In *Numerical Analysis-Theory and Application*; IntechOpen: London, UK, 2011.

50. Tran, D.-D.; Vafaeipour, M.; El Baghdadi, M.; Barrero, R.; Van Mierlo, J.; Hegazy, O. Thorough state-of-the-art analysis of electric and hybrid vehicle powertrains: Topologies and integrated energy management strategies. *Renew. Sustain. Energy Rev.* **2019**, *119*, 109596. [[CrossRef](#)]
51. Hegazy, O.; Barrero, R.; Van Mierlo, J.; Lataire, P.; Omar, N.; Coosemans, T. An advanced power electronics interface for electric vehicles applications. *IEEE Trans. Power Electron.* **2013**, *28*, 5508–5521. [[CrossRef](#)]
52. Druant, J.; Vansompel, H.; De Belie, F.; Sergeant, P. Optimal control for a hybrid excited dual mechanical port electric machine. *IEEE Trans. Energy Convers.* **2017**, *32*, 599–607. [[CrossRef](#)]
53. Druant, J.; Vansompel, H.; De Belie, F.; Melkebeek, J.; Sergeant, P. Torque analysis on a double rotor electrical variable transmission with hybrid excitation. *IEEE Trans. Ind. Electron.* **2016**, *64*, 60–68. [[CrossRef](#)]
54. Delprat, S.; Lauber, J.; Guerra, T.-M.; Rimaux, J. Control of a parallel hybrid powertrain: Optimal control. *IEEE Trans. Veh. Technol.* **2004**, *53*, 872–881. [[CrossRef](#)]
55. Koprubasi, K. *Modeling and Control of a Hybrid-Electric Vehicle for Drivability and Fuel Economy Improvements*; The Ohio State University: Columbus, OH, USA, 2008.
56. Serrao, L.; Onori, S.; Rizzoni, G. ECMS as a realization of Pontryagin’s minimum principle for HEV control. In Proceedings of the American Control Conference, St. Louis, MO, USA, 10–12 June 2009; pp. 3964–3969.
57. Serrao, L.; Onori, S.; Rizzoni, G. A comparative analysis of energy management strategies for hybrid electric vehicles. *J. Dyn. Syst. Meas. Control* **2011**, *133*, 031012. [[CrossRef](#)]
58. Qiu, L.; Qian, L.; Zomorodi, H.; Pisu, P. Design and optimization of equivalent consumption minimization strategy for 4WD hybrid electric vehicles incorporating vehicle connectivity. *Sci. China Technol. Sci.* **2018**, *61*, 147–157. [[CrossRef](#)]
59. Mi, C.; Masrur, M.A. *Hybrid Electric Vehicles: Principles and Applications with Practical Perspectives*; John Wiley & Sons: Hoboken, NJ, USA, 2017.
60. Vafaeipour, M.; Rahbari, O.; Rosen, M.A.; Fazelpour, F.; Ansarirad, P. Application of sliding window technique for prediction of wind velocity time series. *Int. J. Energy Environ. Eng.* **2014**, *5*, 105. [[CrossRef](#)]
61. Verbelen, F. *A Comparative Study of Mechanical and Electrical Variable Transmissions*; Ghent University: Ghent, Belgium, 2019.
62. Caramia, G.; Cavina, N.; Caggiano, M.; Patassa, S.; Moro, D. Battery state of charge management strategies for a real-time controller of a plug-in hybrid electric vehicle. *Energy Procedia* **2018**, *148*, 258–265. [[CrossRef](#)]



© 2020 by the authors. Licensee MDPI, Basel, Switzerland. This article is an open access article distributed under the terms and conditions of the Creative Commons Attribution (CC BY) license (<http://creativecommons.org/licenses/by/4.0/>).